



The Effectiveness of Incorporating Hybrid Reinforcement Nanoparticles in the Enhancement of the Tribological Behavior of Aluminum Metal Matrix Composites

ESSAM B. MOUSTAFA ^{1,6}, WAHEED SAMI ABUSHANAB,²
A. MELAIBARI,^{2,3} OLGA YAKOVITSEVA,⁴ and AHMED O. MOSLEH^{4,5}

1.—Mechanical Engineering Department, Faculty of Engineering, King Abdulaziz University, P.O. Box 80204, Jeddah, Saudi Arabia. 2.—Marine Engineering Department, Faculty of Maritime Studies and Marine Engineering, King Abdulaziz University, Jeddah 21589, Saudi Arabia. 3.—Center of Nanotechnology, King Abdulaziz University, Jeddah 21589, Saudi Arabia. 4.—National University of Science and Technology “MISIS”, Leninsky Prospekt, 4, Moscow, Russian Federation 119049. 5.—Mechanical Engineering Department, Shoubra Faculty of Engineering, Benha University, Cairo 11629, Egypt. 6.—e-mail: abmostafa@kau.edu.sa

Hybrid Al-based surface nanocomposites were manufactured and investigated for industrial applications. The friction stir process (FSP) was successfully utilized to combine and incorporate AA6061 wrought sheets with different reinforcement nanoparticles: silicon carbide (SiC), solid lubricant graphene nanoplates (GNPs), and aluminum oxide (Al_2O_3). Tribological tests were utilized to assess the friction coefficient and wear resistance of the fabricated nanocomposites. The results showed that the AA6061/SiC_GNPs hybrid nanocomposite exhibited ultra-refined grains inside the processed zone with excellent wear resistance behavior. Hence, during the FSP, there was a 36-fold decrease in grain size. Furthermore, the wear rates by volume and mass losses were reduced by 46% and 90%, respectively, due to the self-lubrication properties of the GNPs combined with the SiC particles. Moreover, the friction coefficient of the hybrid AA6061/SiC_GNPs decreased by 30%. The SiC nanoparticles eliminate the negative effect of the GNPs on the hardness. Thus, achieving a balance between improving wear resistance rates and the surface hardness of the manufactured nanocomposites is one of the essential objectives of the study.

INTRODUCTION

Aluminum alloys and their advanced composites are interesting materials because of their excellent physical and mechanical properties, making them applicable to the automotive and aerospace defense industries.¹ However, these alloys are restricted in such applications due to their low surface hardness and poor wear behavior.² This limitation can be resolved by adding different reinforcements, such as SiC, Al_2O_3 , BN, and B_4C to improve the wear and hardness properties.^{3–6} Also, these additives have

low densities and low costs. The AA6061 alloy has been reinforced with SiC and Al_2O_3 particles using the FSP method; these particles were observed to have a good dispersion in the composite matrix.^{7–11} Rajesh et al.⁹ studied the effect of using SiC and Al_2O_3 particles to reinforce aluminum hybrid composites. Increasing the rotating speed led to a rise in the surface temperature, which in turn resulted in the surface being softer and generating further wear. The hardness properties were improved in the mono-composite containing pure SiC, while the wear resistance decreased as the Al_2O_3 content increased; these results were consistent with a previous study.¹²

(Received June 11, 2021; accepted September 28, 2021;
published online October 21, 2021)

Graphene has a high aspect ratio, good mechanical and thermal characteristics, and a low weight, making it ideal for reinforcing aluminum alloys. Graphene's large surface area provides a means to enhance the contact between the metal matrix and the substrate.^{13–17} In general, researchers have used graphene nanoplates (GNPs) to enhance the mechanical characteristics of Al–matrix composites. However, there are few studies on the tribological characteristics of hybrid GNPs/metal matrix composites. GNPs are critical self-lubricating metal materials in composites,^{18–20} and the use of hybrid particles as reinforcements will make it possible to improve the characteristics of the composites. Hybrid metal matrix nanocomposites can be reinforced by adding two or more reinforcements to strengthen the metal matrix alloy.^{21–25} The tribological behavior of hybrid metal matrix nanocomposites is superior to that of the matrix of monolithic nanocomposites. It is known that the particle size of Al₂O₃ nanoparticles significantly affects the wear rate resistance of a nanocomposite matrix.²⁶ A metal matrix copper-based composite has been reinforced with hybrid SiC and graphite using a stir-casting process.

The friction stir process (FSP) is considered to be one of the most advanced approaches employed to produce a surface composite matrix. Moreover, it is deemed efficient for producing thoroughly homogenized stirring nanocomposite materials.^{27,28} The most critical step in FSP is choosing the appropriate processing parameters, i.e., the transverse speed, rotational speed, and tool design. For example, the surface of an AA6061/B₄C composite was fabricated by FSP and showed high wear resistance at multiple processed passes with refined microstructure grains.²⁹

Improving the wear resistance of aluminum alloys and their composites is an important goal and one of the most challenging tasks for researchers; therefore, it has been the focus of several studies. Reinforcement particles have been used in mono- and hybrid combinations to improve aluminum composites.^{30–33} However, many studies have made limited comparisons of the reinforcement elements used to strengthen the aluminum matrix. Enhancement in wear behavior was noticed when a base matrix Al–Si alloy was reinforced with chromium and silicon carbide particles which considerably reduced scratching on the composite surface due to their excellent hardness properties.³⁴

Additionally, GNPs and SiC have been individually investigated in previous studies which used two different reinforcement approaches with various morphologies that were expected to improve the tribological and microstructure behavior of the composites. The present work aimed to improve the wear resistance and hardness behavior of an AA6061 cold-rolled wrought aluminum alloy by fabricating hybrid nanocomposites with a hard self-lubricant surface. The base matrix of AA6061

was reinforced with SiC, GNPs, and Al₂O₃, using the FSP technique. Moreover, this study investigated the role of SiC nanoparticles in balancing the negative effect of the graphene reinforcement particles on the hardness behavior of composites.

MATERIALS AND EXPERIMENTAL WORK

Commercial AA6061 alloy-rolled plates (chemical composition: 0.54 wt.% Si, 0.3 wt.% Fe, 0.24 wt.% Cu, 0.83 wt.% Mg, 0.18 wt.% Cr, and the remainder Al) were selected as the base matrix because of their varied applications. SiC, GNPs, and Al₂O₃ nanoparticles were used as reinforcement nanoceramics on the surface of the base alloy. The reinforcement nanoparticles were chosen based on their ability to improve wear resistance and hardness behavior. The hybrid composites were fabricated using an equal volume content ratio; hence, the first composite contained 50% SiC and 50% GNPs, while the second composite had 50% SiC and 50% Al₂O₃. It is known that superior strengthening can be achieved by combining two types of reinforcement particles, rather than using only a single type.³⁵

The FSP was utilized for fabricating the nanocomposite surface of the aluminum plates, which were prepared and machined using a milling machine to ensure that the set of holes formed a linear pattern, as shown in Fig. 1a. The reinforcement nanoparticles were inserted into the cavities according to two scenarios: the first utilized a pure mono-composite of AA6061/SiC, and the second investigated the impact of SiC nanoparticles on AA6061/GNPs_SiC and AA6061/SiC_Al₂O₃ hybrid nanocomposites. The ceramic nanoparticle hybrids were mixed and stirred well before being added to the base matrix. Furthermore, the hybrids were equally divided and added to the mixture before insertion into the holes of the base matrix. Figure 1b illustrates the FSP fabrication process of the nanocomposite surface. The process was performed using an automatic milling machine with the following conditions: a rotational tool speed of 1120 rpm, a linear travelling speed rate of 30 mm/min, and a fixed tilt angle of 1°.

Transmission electron microscopy (TEM; JSM-200F; JEOL, Tokyo, Japan) was utilized to analyze the SiC, Al₂O₃, and GNP nanoceramics. The powders were well dispersed in a mixture of ethyl alcohol/deionized water using an ultrasonic bath (CPX5800H-E; Branson, USA), and the sample was then loaded onto a 200-mesh carbon grid coated with copper. Figure 2 shows the microstructure and nanostructure of the reinforcement particles. The TEM analyses show the different morphologies of the nanomaterials. The GNPs were characterized by a wide, thin, plate-like surface. The SiC and Al₂O₃ had a similar structural appearance but were characterized by bulky spheres. The average particle sizes of the Al₂O₃ and SiC were 11.3 ± 2 nm and 28 ± 3.5 nm, respectively, whereas the size of the GNPs was 7 ± 1.6 nm thick and 5 ± 0.2 μm wide.

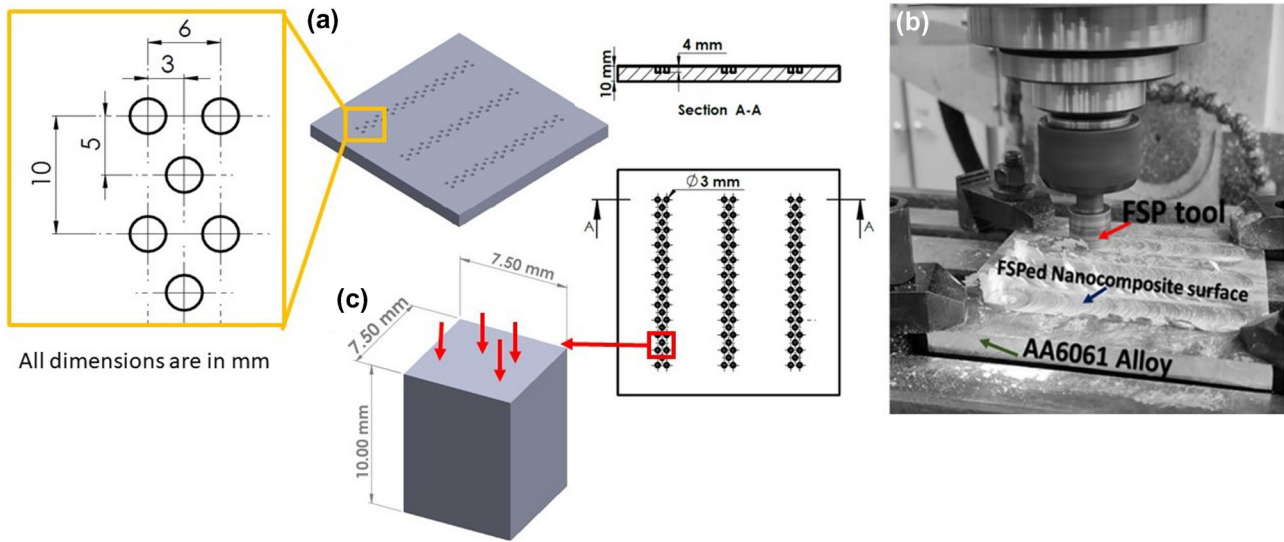


Fig. 1. AA6061 alloy sheets: preparation, holes creation, and manufacturing: (a) schematic of the design of the grooved holes, (b) FSP fabrication process of the surface nanocomposite, and (c) schematic of the wear sample.

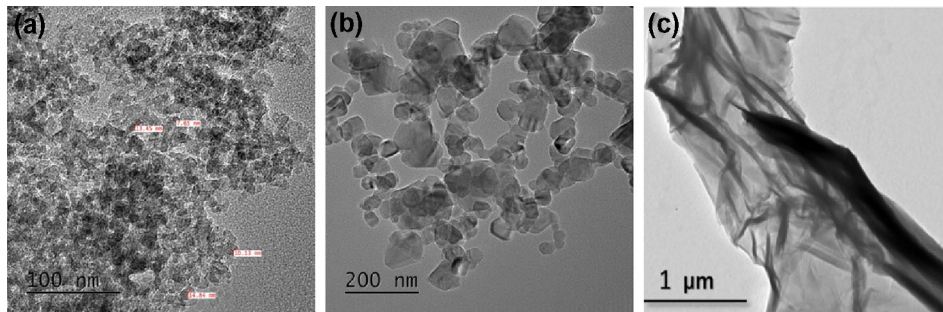


Fig. 2. TEM images of the reinforcement nanoparticles: (a) Al_2O_3 , (b) SiC, and (c) GNPs.

The alumina nanoparticles were found to have a crystalline polymorphic phase, $\alpha\text{-Al}_2\text{O}_3$, and appeared as a white powder. In contrast, the SiC silicon carbide nanoparticles had a cubic morphology and appeared as a grayish–white powder, as observed by the TEM analysis. Due to these differences in particle morphology, the hybridization between the aforementioned reinforcements significantly enhanced the tribological and hardness behavior.

The microstructure examination was carried out before and after the processing by sectioning the samples into dimensions of $20 \times 10 \times 10$ mm across the processing direction. The specimens were subjected to mechanical grinding and polishing, followed by etching using metallurgical standard agents. The samples were analyzed via optical microscopy (BX51; Olympus, USA) and scanning electron microscopy (SEM) using a Tescan-VEGA3 equipped with an X-MAX80 energy-dispersive spectroscopy (EDS) system. The grain size was measured using the standard linear intercept technique. The wear test was performed using two different methods to investigate the wear behavior of the hybrid composite metal matrix. The first technique

was based on the wear volume loss rate, whereas the second method used the weight loss technique. A pin-on-disc tribometer (TRB-S-DE; CSM Instruments, Switzerland) was used to evaluate the wear behavior of the samples used in the study at ordinary room temperature for the volume loss technique. The pin-on-disc test was performed at a constant normal load of 5 N. The pin travelled linearly at 0.1 cm/s in a radius of 2 mm. The ratio of the normal load and the friction force between the steel pin and the sample was used to calculate the friction coefficient. The pin used was made of steel and coated with 100Cr6 steel. The sample used in this test was a disc, and each test was manually stopped once the sliding distance reached 0.1 m. The coefficient was recorded during the test, and the maximum, minimum, and mean values were calculated. A Stylus Profiler System (Dektak XL; Bruker, Germany) measured the wear volume loss rate at different locations through the wear track. The wear track was examined via an optical microscope at high magnification to observe the wear behavior of the fabricated samples.

The wear weight loss rate was determined using the pin-on-ring method (TNO, Delft, Netherlands). The dimensions of the wear samples were $7.5 \times 7.5 \times 10 \text{ mm}^3$ (Fig. 1c). All samples were polished well using a set of grinding papers of different grades, ranging from 600 to 4000. The wear test was carried out for 10 min at 100 rpm with a 0.3-bar load on a 316 stainless steel counterface cylinder (200 mm in diameter), according to the ASTM G99-04A standard at room temperature. Before each test, the cylinder was cleaned with acetone to eliminate surface contaminants. The wear samples used in this method were pins. In addition, Vickers microhardness tests were performed according to the ASTM E-384-17 standard. The hardness was measured using a Vickers microhardness tester (Zwick-Roell, USA) with a weight of 100 g and a shutter speed of 10 s. For all the samples, the Vickers microhardness profile was taken at the center of the stirred zone (SZ) (the cross-section perpendicular to the process direction), starting from the base metal on the right side and ending at the base metal on the left side, with an equal distance step $\approx 1 \text{ mm}$.

RESULTS AND DISCUSSION

Volume Fraction Calculation

The total volume of the produced composite can be computed using Eqs. 1 and 2:

$$V_C = V_p + V_m \quad (1)$$

$$V_C = \text{projected area of tool} \times L \quad (2)$$

where $V_{c,p,m}$ are the volume of the composite, the reinforcement nanoparticles, and the matrix, and L is the manufactured composites length.

The volume used of the nanoceramics and the matrix can be calculated using Eqs. 3 and 4:

$$V_p = \text{No. of holes} \times \text{volume of each hole} \quad (3)$$

$$V_m = V_c - V_p \quad (4)$$

The volume fraction used for the nanoceramics and the matrix can be calculated using Eqs. 5 and 6:

$$VF_p = \frac{V_p}{V_C} \quad (5)$$

$$VF_m = \frac{V_m}{V_C} \quad (6)$$

where VF_p and m are the volume fractions of the reinforcement nanoparticles and the matrix.

The volume of the nanoceramics particles, V_p , equals 0.42 cm^3 , and the volume of the manufactured composite, V_c , is 3.75 cm^3 ; thus, the volume of the matrix, V_m , equals 3.33 cm^3 . Therefore, the

volume fraction of the reinforced nanoceramics within the matrix is 11.6%.

Microstructure Analysis

Figure 3 shows the impact of the reinforcements on optical micrographs for the base AA6061 aluminum alloy at different regions before and after the FSP. The base matrix exhibited uniaxial elongated grains in the initial state (Fig. 3a). After the FSP was completed, the structure changed and the heat-affected zone (HAZ) and the thermomechanical affected zone (TMAZ) exhibited very distinct thermomechanical histories, and therefore had different microstructure and textural characteristics (Fig. 3b and Area 1). The dynamically recrystallized (DRX) microstructure was obtained through FSP due to the friction and extreme plastic deformation inside the SZ (Area 2). This explains why the SZ comprised more uniform equiaxed refined grains than those in the BM, as presented in Fig. 3a and Area 2, respectively.

Both the TMAZ and HAZ were narrow after the FSP, which was carried out at 30 mm/min and 1120 rpm. Fig. 3e shows the grain size frequency/distribution in the SZ of the investigated alloy. After the FSP, the grains were normally distributed about the mean, with a standard deviation (SD) of $3.4 \mu\text{m}$. In the SZ and TMAZ, DRX was the dominant mode of microstructural evolution. As a result, the SZ exhibited a uniformly fine microstructure, while the TMAZ exhibited an elongated grain structure due to the thermomechanical effect of the stirring action, which has been confirmed by others.³⁶

Figure 4 shows the micrography of the microstructure and the grain size frequency/distribution in the SZ reinforced with SiC, GNPs, and Al_2O_3 . The effectiveness of different reinforcing nanoceramics during the FSP in mono- or hybrid reinforcements decreased the grain size, as observed in Fig. 4a, c, and e. These nanoceramics acted as barriers to grain growth. Reinforcement by including different nanoparticles in the BM by the FSP led to more refinement. The grains were uniformly equiaxed and generally distributed about the mean, with a lower SD (Fig. 4b, d, and f). During the FSP, the dynamic restoration phenomena were significantly influenced by the nanoparticles. These increased the refinement of the grains in the SZ by increasing the number of nucleation sites that are available for new grains, as a result of Zener pinning and particle-stimulated nucleation (PSN) mechanisms, in agreement with previous work.³⁷

The average grain size of the base metal was $250 \pm 40 \mu\text{m}$ with an aspect ratio of length to width = $250:70 \approx 3.6$, as observed in Fig. 4g. After completing the FSP, the stirred zone had an average grain size of $12.5 \pm 3.4 \mu\text{m}$ with nearly equiaxed grains with an aspect ratio of ≈ 1.1 . Adding various reinforcing nanoceramics, such as SiC, SiC_GNPs, and SiC_ Al_2O_3 , led to refinement in the SZ. The average

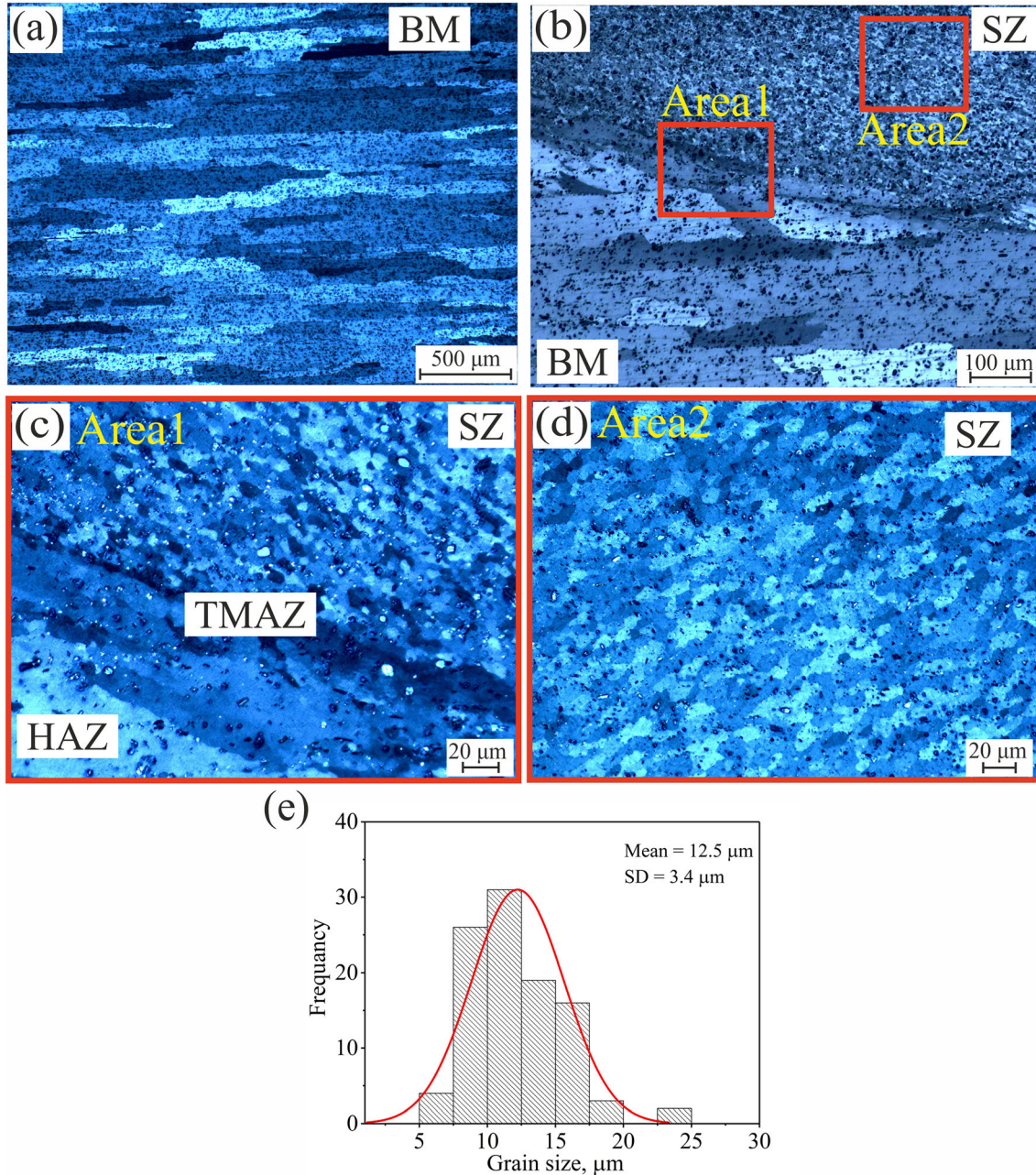


Fig. 3. The microstructure of (a) the as-received AA6061 alloy plates, and (b) the FSP of the investigated alloy at 1120 rpm and 30 mm/min showing two areas, *Area1* and *Area2* (which are enlarged in (c) and (d), respectively), with *Area1* the transition region between the SZ and the BM, and *Area2* the stirred zone; (e) grain size frequency in SZ.

grain sizes in the SZ for SiC, SiC_GNPs, and SiC_{Al₂O₃} were $10.8 \pm 3.6 \mu\text{m}$, $10.4 \pm 2.8 \mu\text{m}$, and $11.5 \pm 2.8 \mu\text{m}$, respectively. The elongated structure of the original alloy became equiaxed and 20 times more refined after the FSP. The grain size decreased 25-fold when the hybrid of SiC and GNPs was used to reinforce the base matrix.

The aspect ratios for the grains in the SZ for SiC, SiC_GNPs, and SiC_{Al₂O₃} were 1.05, 1.04, and 1.05, respectively, confirming homogenous equiaxed grains. The presence of nanoparticles led to an increase in grain refinement in the SZ, which is

attributed to the Zener pinning and the PSN mechanisms. Figure 5 shows the SEM micrographs and the EDS mapping of the SZ of the fabricated surface composite reinforced by a hybrid of SiC_GNPs (Fig. 5a) and SiC_{Al₂O₃} (Fig. 5b). The SEM images show the morphology of the hybrid composites. In general, it is difficult to replicate the ability of the FSP to create a completely homogeneous distribution of the nanoparticles, since the degree of heterogeneity and the severity of agglomeration depend on the nanoparticle type, matrix chemistry, and processing parameters. The EDS

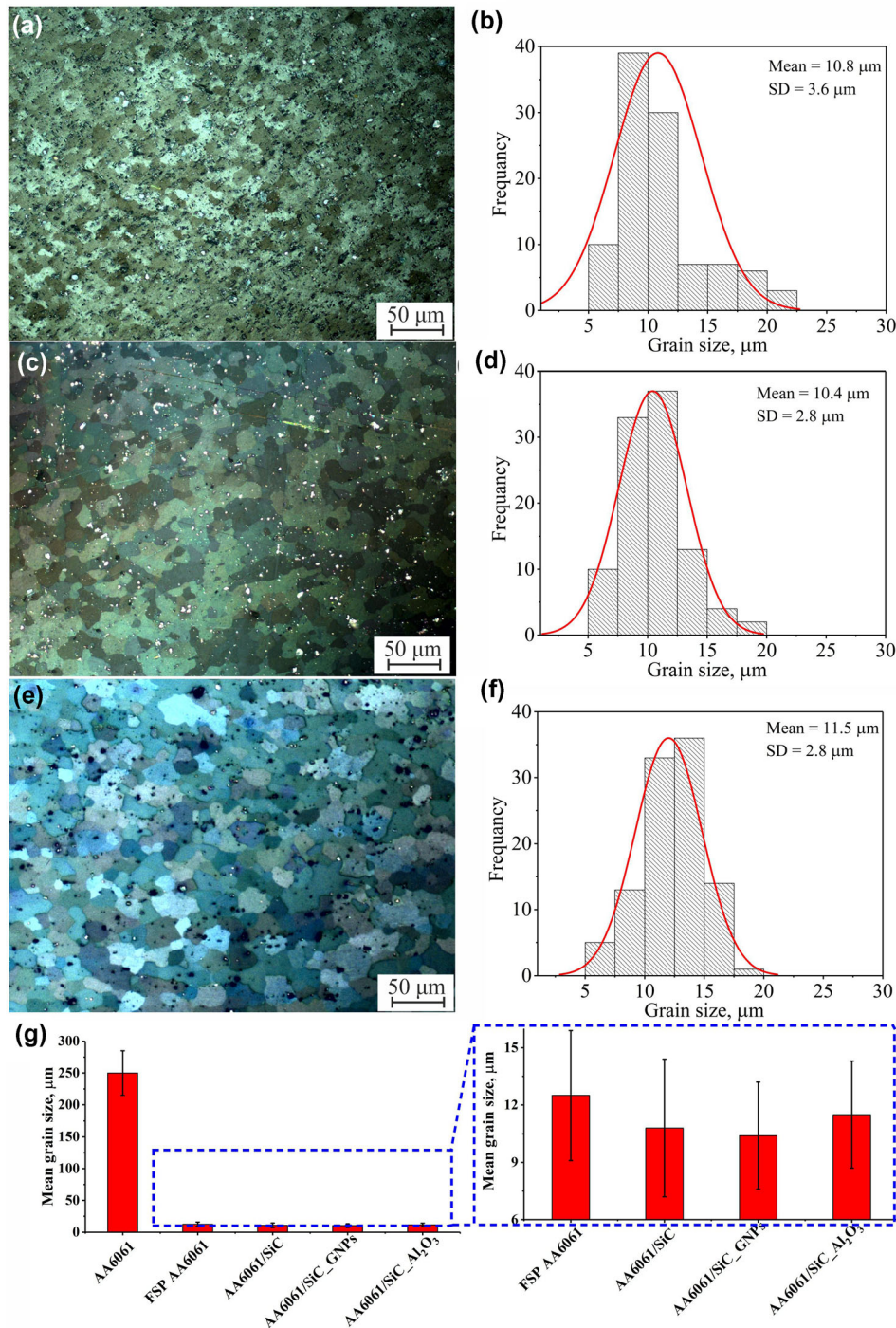


Fig. 4. The microstructure and grain size frequency of the SZ processed at 1120 rpm and 30 mm/min and reinforced with (a, b) SiC, (c, d) a hybrid of SiC_GNPs, (e, f) a hybrid of SiC_Al₂O₃, and (g) average grain size in SZ for different nanocomposites.

maps confirmed the presence of reinforced particles in the SZ, as well as the main alloying elements and phases of the investigated alloy. Generally, in all the samples, it can be observed that the reinforcing nanoparticles were nearly homogeneously distributed in the SZ. The EDS analysis confirmed that Mg₂Si phase particles were formed on the surface of the scanned sample. The white particles that appeared in the microstructure images (Fig. 5a

and b) were related to the formation of the Mg₂Si intermetallic phase, which was also noted in another study.³⁸

Wear Characterization

The friction coefficient increased at the beginning of the test until it reached a specific value, after which it decreased until it reached a steady state.^{39–42} This

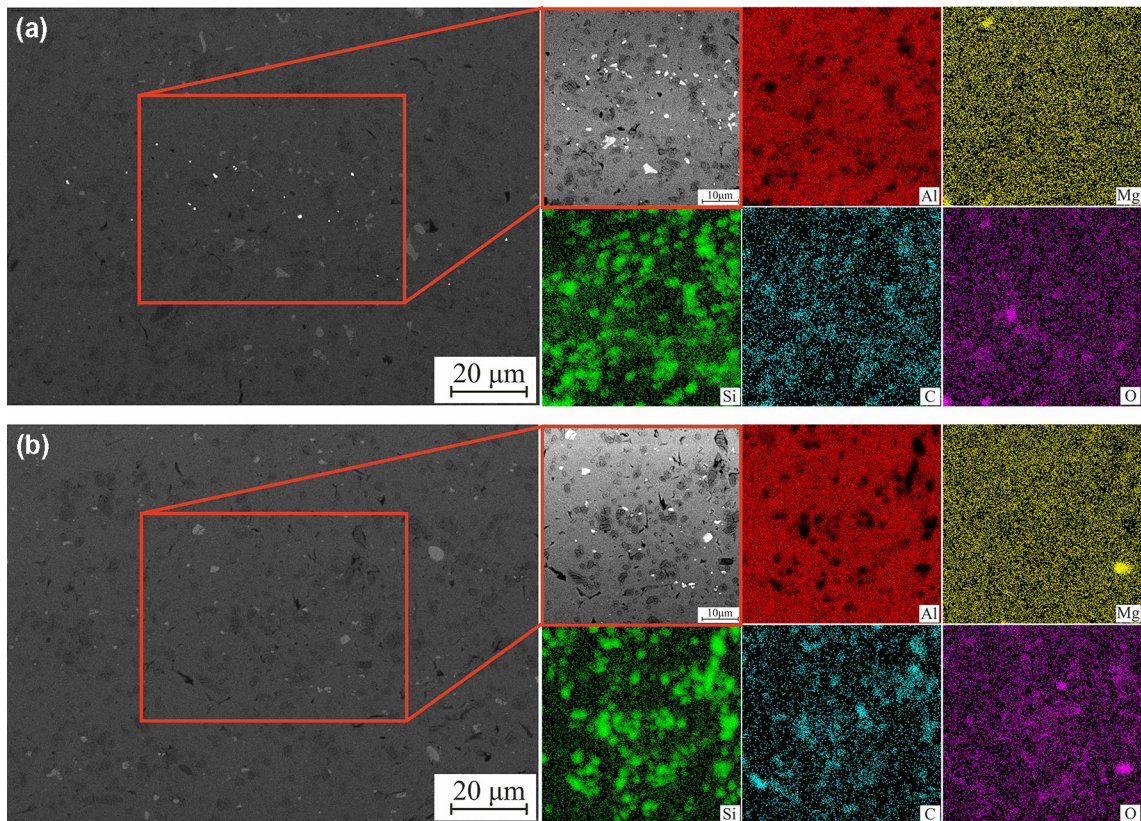


Fig. 5. SEM image and EDS mapping analysis of the SZ of the fabricated surface composite reinforced with a hybrid of (a) SiC_GNPs and (b) SiC₂Al₂O₃.

mechanism can be attributed to the higher adhesive contact between the surface of the tested specimen and the pin of the wear tool. As a result, higher frictional forces were produced when the test began. During the tests, the coefficients of friction were evaluated by measuring fluctuation coefficients. Figure 6a shows the time dependency of the coefficient of friction (COF) for the original and fabricated composites. Table I, in the supplemental materials, contains data on the average coefficient of friction of the base alloy, the surface created by the FSP, the hybrid, and the mono-composite samples.

The average value of the friction coefficients for the mono- and hybrid composite matrixes revealed an inverse relationship between the reinforcement particles and the coefficient of friction. The hybridization of the SiC and Al₂O₃ nanoparticles significantly improved the wear behavior of the fabricated composite metal matrix samples, consistent with other work.^{40,41} The friction coefficient of the hybrid nanocomposite AA6061/SiC_GNPs decreased as the surface roughness decreased, which was contrary to the results in a previous study.⁴² When the aluminum alloy matrix was reinforced with a small amount of graphene GNPs, it exhibited excellent mechanical behavior. In addition to improved sliding properties, it decreased the adhesion and the friction with contacting surfaces; thus, the hybrid nanocomposite AA6061/SiC_GNPs

exhibited the lowest coefficient of friction, 0.48, when compared with the base metal and other composites. Furthermore, by squeezing out these particles on the composite surface, a protective film between the tribo-pair surfaces was formed and the GNPs were generated, which led to a reduction in the adhesive wear mechanism, in accordance with previous work.⁴³ Consequently, the COF of the hybrid nanocomposite AA6061/SiC_GNPs was reduced.

Figure 6b shows a comparison between the mono- and hybrid composite variations measured with a surface profiler. The hybrid composite achieved the lowest depth in the current study. This may be because of its greater wear strength and the excellent dispersion of such hybrids in the aluminum base matrix of the reinforcing nanoparticles. On the other hand, lower wear resistance was observed for the base AA6061 alloy and the AA6061-FSP alloy was. Figure 6c shows a comparison between the results of the wear volume loss for all the samples. The hybrid samples of AA6061/SiC_GNPs and AA6061/SiC₂Al₂O₃ exhibited low wear volume losses of approximately 0.207 mm³ and 0.224 mm³, while the most wear volume loss value was observed for the base AA6061, at a value of 0.38 mm³. Thus, the volume loss decreased as a result of the FSP for the AA6061/SiC, AA6061/SiC_GNPs, and AA6061/SiC₂Al₂O₃ when compared with the base alloy by

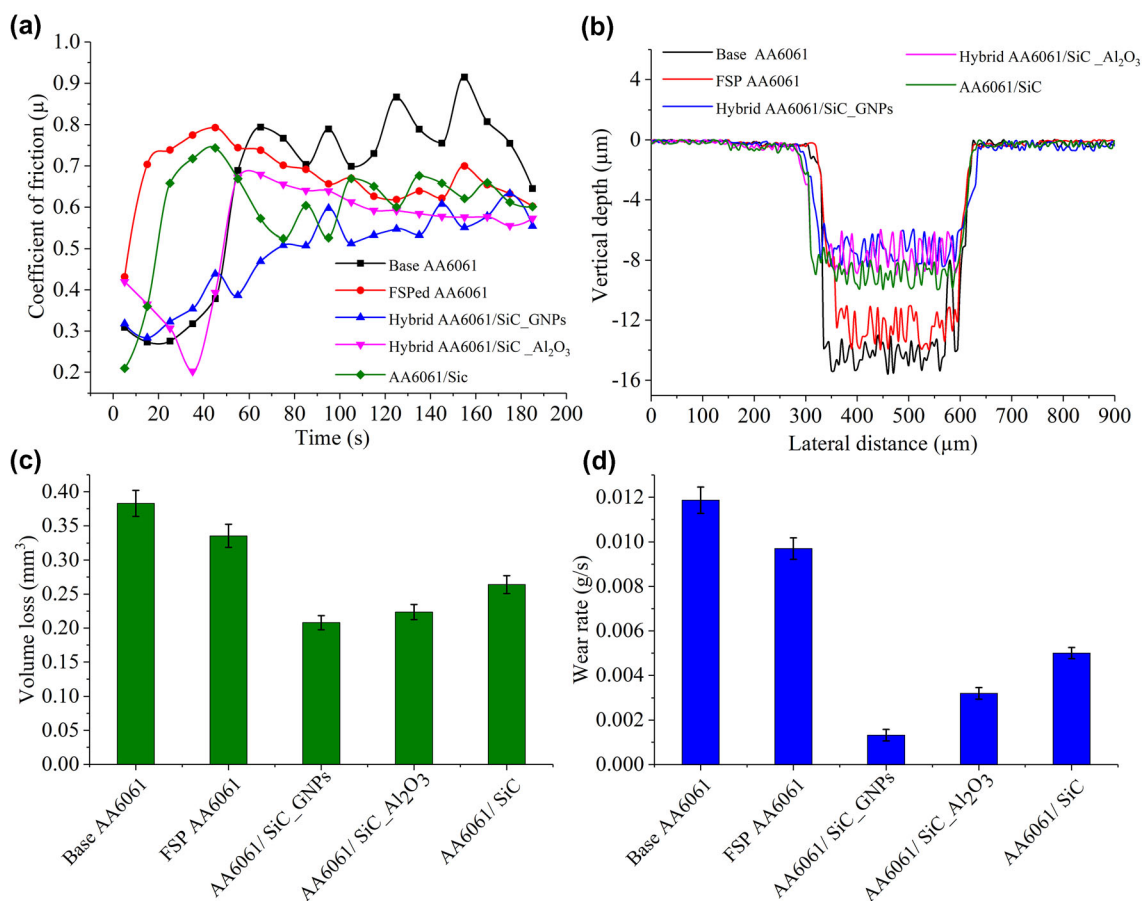


Fig. 6. (a) Average friction coefficient, (b) vertical depth obtained by surface profiler test, (c) wear volume loss, and (d) wear rate by mass loss of the base and fabricated composites.

13%, 31%, 46%, and 42%, respectively. The basic matrix and samples that had undergone the FSP had larger wear tracks than the nanocomposite-containing hybrid nanoparticles. Due to the adhesive frictional force between the tool pin and the base alloy, a rough surface morphology was generated during the wear test. The composite surface had fewer asperities than the worn surface, which may be attributed to the impact of the reinforcing particles in providing high strength and hardness. The wear rate due to the weight loss was calculated from (Eqs. 7 and 8):⁴³

$$W_n = W_0 - W_f \quad (7)$$

$$\text{Wear rate} = \frac{W_n}{t} \quad (8)$$

where W_0 and W_f are the sample weights before and after the wear test. W_n is the net sample weight, and t is the time of the wear test. The wear rate results were in line with the wear volume loss results.

Figure 6d shows the higher wear rate of the base AA6061 alloy compared to the other samples. Evidently, the reinforcement nanoparticles had a significant impact on the wear behavior of the AA6061

alloy. The hybrid AA6061/SiC GNP and AA6061/SiC Al₂O₃ samples had the lowest wear rate among those investigated, which may be attributed to the homogeneity of the base matrix and the excellent dispersion of the reinforcement nanoparticles. The wear volume loss was deduced from the surface profiler data and the optical microscope images of the worn samples. The mass loss decreases as a result of the FSP for the AA6061/SiC, AA6061/SiC_GNPs, and AA6061/SiC_Al₂O₃ were 20%, 60%, 90%, and 75% of the mass of the base material, respectively.⁴³

Graphene nanoplates have a soft nature. The incorporation of GNP along with SiC improved the tribological behavior of the investigated alloy. A section of a graphene nanoplate can be stuck on the surface during block-on-ring-wear and pin-on-disc tests (Fig. 7). The sticky parts of the GNP on the surface create a lubricated surface, increasing wear resistance. Additionally, GNP with multiple layers exhibit weak van der Waals bonds, resulting in easy sliding under shear loads, making the composite self-lubricating.^{44,45} Thus, on the worn surface, the GNP squeeze out and smudge (Fig. 7c). As a result of this action, the wear properties of the nanocomposites containing GNP improved.

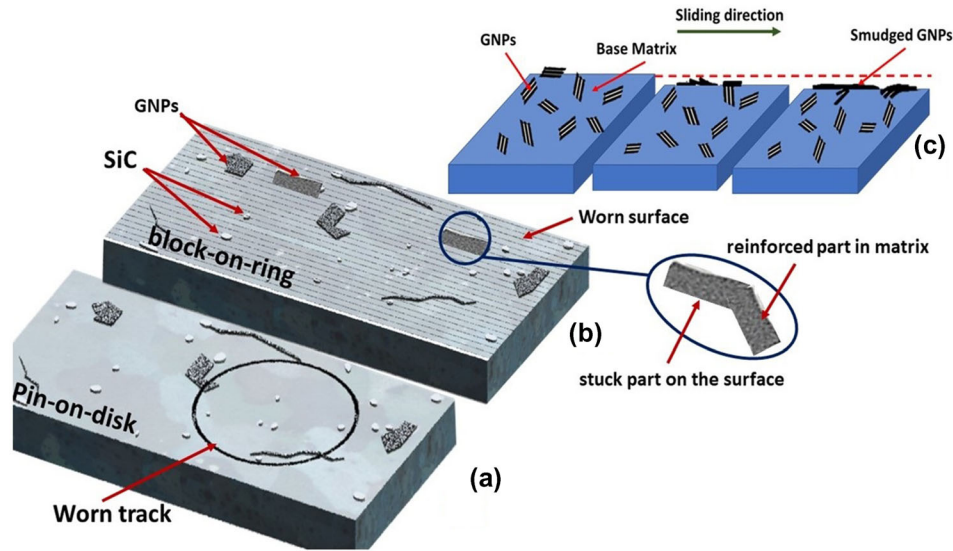


Fig. 7. Schematics of the wear test process: (a) pin-on-disk using the tribometer tester (volume loss), (b) block-on-ring wear test (weight loss), and (c) squeezed out and smudged GNPs on the surface of the fabricated nanocomposite.

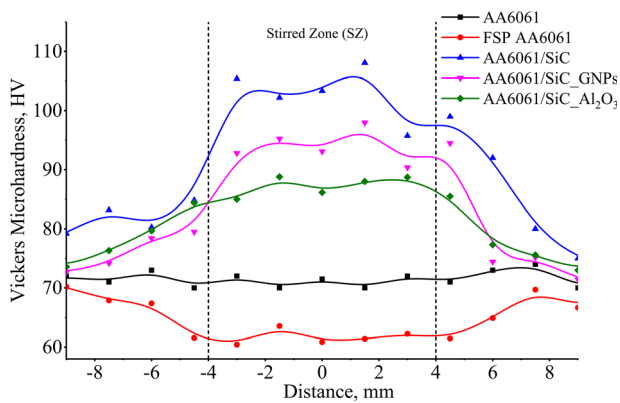


Fig. 8. Vickers microhardness profile of the investigated samples.

Microhardness Evaluation

The microhardness of composite materials is considered an intrinsic property because it depends only on composition and microstructure. However, abrasion wear resistance is not considered an inherent property because it may depend on different parameters, such as the wear test method, the abrasive properties, and the environmental and operating conditions. Figure 8 shows the Vickers microhardness profile across the samples for the base AA6061 alloy and the SZ for different reinforced nanocomposites. The average Vickers microhardness of the original alloy was 72 = HV. After FSP, the average hardness in the SZ was 62 HV. The hardness improved in the SZ after FSP when the samples were reinforced with various nanoceramics. This enhancement in hardness may be attributed to the refinement of the alloy matrix and the uniform dispersion of hard nanoceramics into the matrix. The average measured hardness in the surfaces' SZ composite layers reinforced with

SiC, SiC_GNPs, and SiC_{Al₂O₃} were 106, 95, and 88 HV, respectively. Therefore, the hardnesses were enhanced by 50%, 40%, and 25% by compositing the surface with SiC, SiC_GNPs, and SiC_{Al₂O₃}, respectively.

The dispersion of reinforced particles depends on the processing parameters of FSP and the type of the reinforced particles, so the hardness behavior may vary in the stirred zone. Although the reinforcement particles' prediction behavior increases such composite hardness, the results revealed that the hardness has not significantly improved. The hardness value can be attributed to the distribution of the reinforcement nanoparticles within the aluminum base matrix, and the nanoparticles are not usually entirely distributed by FSP. These results were consistent with those from previous studies.^{46,47} Additional graphene content in the composite matrix tends to negatively impact mechanical properties due to graphene's soft nature. The SiC particles were added with graphite to the hybrid composite to improve its mechanical properties by balancing the negative effect of the graphene particles; the results were consistent with a previous study.²⁶ The inverse relationship between hardness and wear resistance can also be attributed to the soft nature of the graphene nanoplates, which leads to improved wear resistance properties; however, the mechanical and hardness behavior are not significantly improved. These results are also consistent with a previous study.⁴⁸ A proportional increase in the wear resistance rate with an increase in hardness is generally observed with metal matrix composites containing multi-phase intermetallic compounds. However, in the current study, the ceramic reinforcement nanoparticles did not entirely fuse in the base matrix; thus, their

morphology produced different results for the wear and hardness tests.

CONCLUSION

Mono- and hybrid nanocomposites were successfully fabricated via the FSP technique. AA6061 rolled plates were the base metal matrix, and SiC, Al₂O₃, and GNPs were used as the reinforcement nanoparticles. Al₂O₃ nanoparticles and GNPs, which differ in their properties and structures, were incorporated with SiC nanoparticles to explore an appropriate hybrid composite that resists wear with adequate hardness behavior. Microstructure, wear behavior, and the hardness of the original sheets, the FSP-treated samples, and the fabricated composites were studied. From the results, we can conclude that:

- The base alloy showed elongated microstructure grains due to the rolling process; after FSP, the elongated structure became equiaxed and refined 20-fold. The reinforcement of the aluminum base using different nanoceramic particles led to an increase in grain refinement. The grain size decreased 25-fold when the hybrid of SiC and GNPs was used to reinforce the base matrix.
- The hybrid composites containing SiC and other reinforcement particles (GNPs and Al₂O₃) provided the hybrid composite matrix with a superior wear resistance compared to the monocomposite and base matrix. The GNPs showed a significant enhancement in wear resistance due to their morphological and self-lubricating properties. The hybrid nanocomposite achieved as much as a 40% improvement over the properties of the base alloy.
- The hardened surface of the original AA6061 rolled plates softened in the SZ after FSP by 15%. The hardnesses of the composite surfaces composed of SiC, SiC_GPNs, and SiC_Al₂O₃ improved by 50%, 40%, and 25%, respectively. The relationship between hardness and resistance to wear was not reliable when investigating and comparing the mono- and hybrid composites.
- Including SiC nanoparticles with the GNPs increased the mechanical properties of the samples by balancing the negative effect of the GNPs, and the overall results revealed that the hybrid SiC_GPNs nanocomposite matrix achieved good wear resistance and desirable hardness behavior.

ACKNOWLEDGEMENTS

This Project was funded by the deanship of scientific research (DSR) at King Abdulaziz University, Jeddah under Grant No. (RG-3-150-38). The authors therefore gratefully acknowledges technical and financial support from DSR.

CONFLICT OF INTEREST

The authors declare that they have no conflict of interest.

SUPPLEMENTARY INFORMATION

The online version contains supplementary material available at <https://doi.org/10.1007/s11837-021-04955-w>.

REFERENCES

1. A.K. Sharma, R. Bhandari, A. Aherwar, R. Rimašauskienė, and C. Pinca-Bretotean, *Mater. Today Proc.* 26, 2419. (2020).
2. I. Sudhakar, V. Madhu, G.M. Reddy, and K.S. Rao, *Def. Technol.* 11, 10. (2015).
3. D. Aruri, K. Adepu, K. Adepu, and K. Bazavada, *J. Mater. Res. Technol.* 2, 362. (2013).
4. W. Chao, X. Xiangxin, C. Xiaozhou, Y. He, and C. Gongjin, *Arch. Metall. Mater.* 58, 509. (2013).
5. C. Xiaozhou, W. Chao, X. Xiangxin, and C. Gongjin, *Arch. Metall. Mater.* 60, 2493. (2015).
6. W.S. Abushanab, E.B. Moustafa, A.A. Melaibari, A.D. Kotov, and A.O. Mosleh, *Coatings* 11, 977. (2021).
7. W.S. Abushanab, and E.B. Moustafa, *J. Mater. Res. Technol.* 9, 7460. (2020).
8. E. Moustafa, *Materials* 10, 1053. (2017).
9. S.M. Essam, B. Moustafa, S. Abdel-Wanis, and T. Mahmoud, *J. Mater. Sci. Surf. Eng.* 5, 524. (2017).
10. M.E.B., *Materials (Basel)*, 11 (2018).
11. E.B. Moustafa, and A.O. Mosleh, *J. Alloys Compd.* 823, 153745. (2020).
12. S.S.A. Aziz, H. Abulkhair, and E.B. Moustafa, *J. Mater. Res. Technol.* 13, 1275. (2021).
13. S. Mondal, *Metal. Mater. Int.* (2020).
14. M. Rashad, F. Pan, A. Tang, and M. Asif, *Progr. Nat. Sci. Mater. Int.* 24, 101. (2014).
15. M.C. Şenel, M. Gürbüz, and E. Koç, *J. Compos. Mater.* 53, 4043. (2019).
16. A.S. Zayed, B.M. Kamel, T.A. Osman, O.A. Elkady, and S. Ali, *Fuller. Nanotub. Carbon Nanostruct.* 27, 538. (2019).
17. E.B. Moustafa, and M.A. Taha, *Appl. Phys. A* 126, 220. (2020).
18. A.D. Moghadam, B.F. Schultz, J.B. Ferguson, E. Omrani, P.K. Rohatgi, and N. Gupta, *JOM* 66, 872. (2014).
19. M. Tabandeh-Khorshid, E. Omrani, P.L. Menezes, and P.K. Rohatgi, *Eng. Sci. Technol.* 19, 463. (2016).
20. Y. Su, Y. Zhang, J. Song, and L. Hu, *Wear* 372–373, 130. (2017).
21. S. Gobikannan, and S. Gopalakannan, *Appl. Mech. Mater.* 852, 110. (2016).
22. H.I. Kurt, M. Oduncuoglu, and R. Asmatulu, *J. Iron Steel Res. Int.* 23, 1119. (2016).
23. N. Pol, G. Verma, R.P. Pandey, and T. Shanmugasundaram, *Def. Technol.* 15, 363. (2019).
24. P. Pugalenthi, M. Jayaraman, and V. Subburam, *Mater. Tehnol.* 53, 49. (2019).
25. B.N. Sarada, P.L.S. Murthy, and G. Ugrasen, *Mater. Today Proc.* 2, 2878. (2015).
26. D.M. Shinde, P. Sahoo, and J.P. Davim, *Adv. Compos. Lett.* 29, 1. (2020).
27. S.M. Essam, B. Moustafa, S. Abdel-Wanis, T. Mahmoud, and E.-S. El-Kady, *Am. Sci. Res. J. Eng. Technol. Sci.* 22, 98. (2016).
28. V. Sharma, U. Prakash, and B.V.M. Kumar, *J. Mater. Process. Technol.* 224, 117. (2015).
29. K.M. Mehta, and V.J. Badheka, *Wear* 426–427, 975. (2019).

30. M. Akbari, M.H. Shojaeefard, P. Asadi, and A. Khalkhali, *J. Mater. Design Appl.* 233, 790. (2017).
31. M.A. Ezazi, M.M. Quazi, E. Zalnezhad, and A.A.D. Sarhan, *Ceram. Int.* 40, 15603. (2014).
32. E.R.I. Mahmoud, M. Takahashi, T. Shibayanagi, and K. Ikeuchi, *Wear* 268, 1111. (2010).
33. N. Yuvaraj, S. Aravindan, and Vipin, *Trans. Indian Inst. Metals* 70, 1111. (2016).
34. J. Kumar, D. Singh, N.S. Kalsi, S. Sharma, C.I. Pruncu, D.Y. Pimenov, K.V. Rao, and W. Kapłonek, *J. Mater. Res. Technol.* 9, 13607. (2020).
35. A. Heidarzadeh, S. Mironov, R. Kaibyshev, G. Çam, A. Simar, A. Gerlich, F. Khodabakhshi, A. Mostafaei, D.P. Field, J.D. Robson, A. Deschamps, and P.J. Withers, *Progr. Mater. Sci.* 117, 100752. (2021).
36. M. Yang, C. Xu, C. Wu, K.-C. Lin, Y.J. Chao, and L. An, *J. Mater. Sci.* 45, 4431. (2010).
37. J. Wang, Y. Lu, D. Zhou, Y. Zhang, Z. Bai, and X. Li, *Mater. Res. Express* 6, 126577. (2019).
38. E. Linardi, R. Haddad, and L. Lanzani, *Proc. Mater. Sci.* 1, 550. (2012).
39. A. Abbas, and S.-J. Huang, *JOM* 72, 2272. (2020).
40. B. Ballóková, L. Falat, V. Puchý, Z. Molčanová, M. Besterčí, R. Džunda, A. Abbas, and S.-J. Huang, *Materials* 13, 2688. (2020).
41. A. Abbas, S.J. Huang, B. Ballóková, and K. Sülleiová, *Tribol. Int.* 142, 105982. (2020).
42. S.J. Huang, A. Abbas, and B. Ballóková, *J. Mater. Res. Technol.* 8, 4273. (2019).
43. E.B. Moustafa, A. Melaibari, and M. Basha, *Ceram. Int.* 46, 16938. (2020).
44. J. Yang, Y. Xia, H. Song, B. Chen, and Z. Zhang, *Tribol. Int.* 105, 118. (2017).
45. C. Ornelas, F. Paraguay-Delgado, and J. Lara-Romero, *J. Mater. Res. Technol.* 8, 3672. (2019).
46. D. Yadav, and R. Bauri, *J. Mater. Eng. Perform.* 24, 1116. (2015).
47. N. Gangil, A.N. Siddiquee, and S. Maheshwari, *J. Alloys Compd.* 715, 91. (2017).
48. A.C. Faria, U.M. Benassi, R.C. Rodrigues, R.F. Ribeiro, and G.M. Mda, *Braz. Dent. J.* 18, 60. (2007).

Publisher's Note Springer Nature remains neutral with regard to jurisdictional claims in published maps and institutional affiliations.